Ionic Liquid Crystalline Calixarene with Photo-switchable Proton Conduction

Alberto Concellón, Iván Marín, Joaquín Barberá, Mercedes Marcos, and José L. Serrano*

Instituto de Nanociencia y Materiales de Aragón (INMA), CSIC-University of Zaragoza, 50009 Zaragoza, Spain. Email: joseluis@unizar.es

This paper is dedicated to Professor Robert Deschenaux (Université de Neuchâtel), friend and colleague, on the occasion of his retirement

We have developed a new strategy for the preparation of a light-responsive ionic liquid crystal (LC) that shows photo-switchable proton conduction. The ionic LC consists of a bowl-shaped calix[4]arene core ionically functionalized with azobenzene moieties. The non-covalent architectures were obtained by the formation of ionic salts between the carboxylic acid group of an azo-derivative and the terminal amine groups of a calixarene core. The presence of ionic salts results in a hierarchical self-assembly process that extends to the formation of a nanostructured lamellar LC arrangement (smectic A phase). In this LC phase, the ionic LC calixarene is able to display proton conductive properties, since the ionic nanosegregated areas (formed by the ionic pairs) generate the continuous channels that favor proton transport. The optical and photo-responsive properties were studied by UV-Vis spectroscopy, demonstrating that the azobenzene moieties of the ionic LC undergo reversible *E* to *Z* isomerization by irradiation with UV light. Interestingly, this *E*-to-*Z* photoisomerization results in a decrease of the proton conductivity values since the bent-shaped *Z*-isomer disrupts the lamellar LC phase. This isomerization process is totally reversible and leads to an ionic LC material with unique photo-switchable proton conductive properties.

Keywords: calixarene, azobenzene, ionic liquid crystal, photo-isomerization, proton conductivity.

Introduction

Calixarenes are an important class of macrocycles that offer a wealth of opportunities for materials chemists due to the well-established synthetic procedures for their functionalization, their bowl shape, and their host-guest chemistry.[1-4] Liquid crystal (LC) calixarenes represent an attractive option for the design of functional self-organized materials because they combine the inherent properties of the calixarene macrocycle with the anisotropic properties provided by the LC state.[5-6] LC calixarenes are usually prepared by covalent functionalization of the narrow and/or wide rims of the calixarene with pro-mesogenic units.[7-16] Although supramolecular approaches based on molecular recognition have been less often considered, they provide distinctive advantages rising from the facile but reliable preparation when compared to entirely covalent systems, which usually require time consuming synthetic procedures. Among the different non-covalent interactions that hold molecular components together, ionic self-assembly has recently turned into a powerful and versatile option to create nanostructured LC materials with several interesting properties.[17-19] In fact, ionic LCs have drawn an extensive academic interest in recent times due to the promise of real-world applications in many fields, including biomaterials, catalysis, or ion-conductive materials.[20-26]

Herein, we explore for first time the non-covalent functionalization of a calixarene core to obtain ionic LC materials. Specifically, we prepare a supramolecular ionic complex between the terminal amine groups of tetraamino-calix[4]arene and the carboxylic acid group of an azobenzene derivative (**Scheme 1**). Formation of ionic salts resulted in a hierarchical self-assembly process, wherein the charged sites promote additional self-assembly that extends to the formation of a nanosegregated lamellar LC organization. Such nanosegregated LC phase results from the charge-charge coupling interations and the microphase separation between incompatible polar and apolar parts of the molecule. This leads to ionic nanosegregated areas within the LC phase which form continous ionic channels that enable proton conduction. Additionaly, we introduced an azoderivative as structural controlling element in order to obtain a proton-conducting LC material, in which its proton conductivity can be switched by *E-Z* photoisomerization. In general, the incorporation of azobenzene moieties into LC provides access to promising materials for applications in different fields such as the preparation of photomechanical actuators, photoresponsive surfaces, optical storage media, or light-responsive nanocarriers.[27-34]

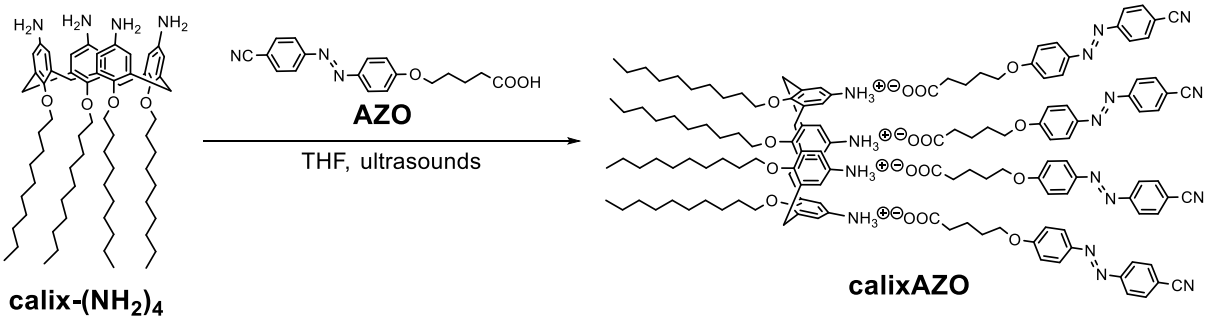

Scheme 1. Synthetic route of Ionic Calix[4]arene (**calixAZO**)

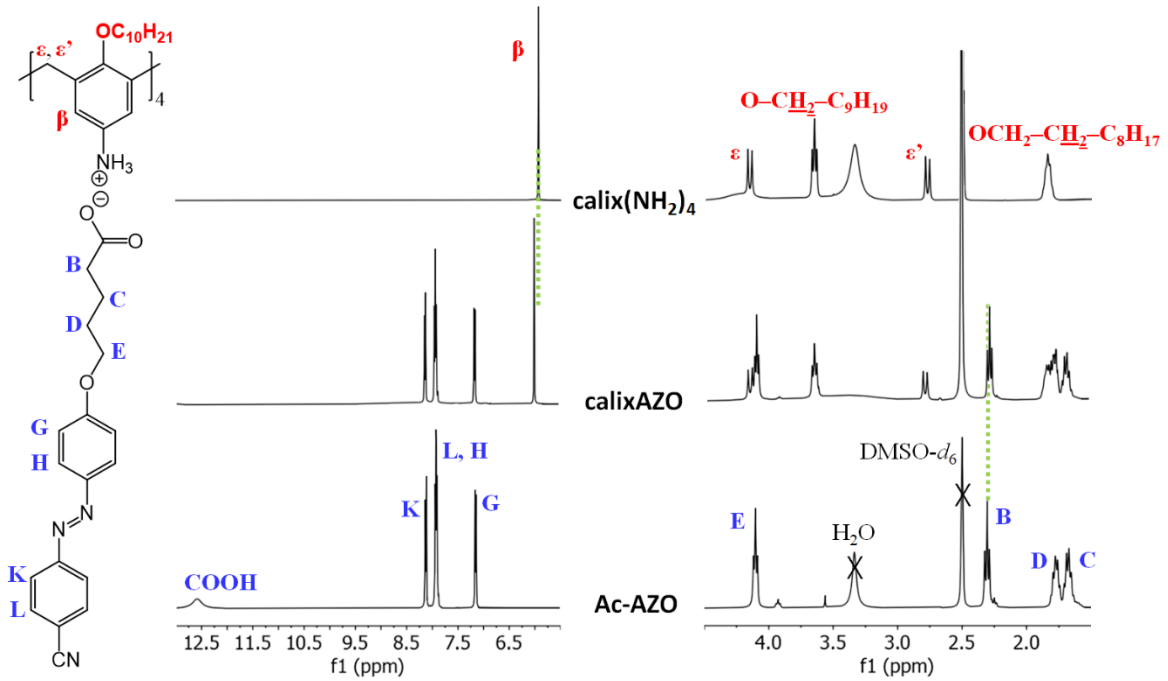

Figure 1. ^{1}H NMR spectra (400 MHz, DMSO-d_6, 298K) of **calix-(NH$_2$)$_4$**, **Ac-AZO**, and **calixAZO**.

Results and Discussion

The ionic calix[4]arene (**calixAZO**) was prepared following a previously-described method.[35-36] Briefly, a solution of 5,11,17,23-tetraamino-25,26,27,28-tetradecyloxycalix[4]arene (**calix(NH$_2$)$_4$**) in tetrahydrofuran (THF) was mixed with a THF solution of 5-(*p*-cyanophenylazophenyloxy)pentanoic acid (**Ac-AZO**) in the stoichiometry necessary to functionalize the four terminal amino groups of the calixarene core (i.e., 1:1 stoichiometry between the carboxylic acid and each terminal amine of the calixarene unit) (**Scheme 1**). The mixture was sonicated for 10 min, then THF was slowly evaporated at room temperature, and dried under vacuum until the weight remained constant.

Formation of the ionic complex was confirmed by nuclear magnetic resonance (NMR) spectroscopy. In the ^{1}H NMR spectrum of **calixAZO**, the proton signal of the carboxylic acid disappeared after the formation of the ionic salts. Likewise, the protons close to the ionic pair also experience changes in their chemical shifts. For instance, the proton signals of the methylene adjacent to the carboxylic acid (H_B) shifted from 2.32 to 2.30 ppm. Moreover, the aromatic protons adjacent to the NH_3^+ group (H_β) moved to lower field (from 5.94 to 5.96 ppm), also confirming the formation of the ion complex. In the ^{13}C NMR spectrum of **calixAZO** the carboxyl group signal (C_A) of the acid shifts from 174.35 to 174.55 ppm, confirming carboxylate (COO^-) formation. Deprotonation of the carboxylic acid was also corroborated by the displacement to a lower field of the methylenic carbons (C_B) close to the carboxylate that shifted from 33.38 to 33.25 ppm.

The thermal stability of **calixAZO** was studied by thermogravimetric analysis (TGA), and the temperature at which there is a 5% weight loss ($T_{5\%}$) was ca. 100 °C above the clearing point. Polarized optical microscopy (POM) and differential scanning calorimetry were used to study the liquid crystal properties. **calixAZO** showed enantiotropic liquid crystal behavior with textures typical of smectic A (SmA) mesophases (**Figure 3a**). Relevant data is gathered in **Table 1**. Although the precursors **calix-(NH$_2$)$_4$** and **Ac-AZO** did not show mesomorphic behavior and are both crystalline materials,[7, 37] it is noteworthy that **calixAZO** displayed a stable enantiotropic LC phase, which also provides evidence for the formation of the ionic complex.

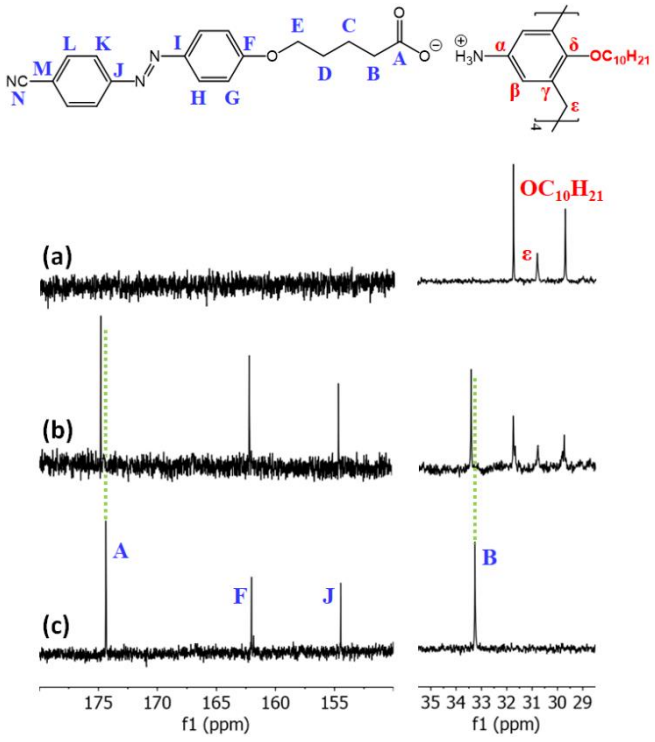

Figure 2. ^{13}C NMR spectra (400 MHz, DMSO-d_6, 298K) of: **(a) calix-(NH$_2$)$_4$**, **(b) calixAZO**, and **(c) Ac-AZO**.

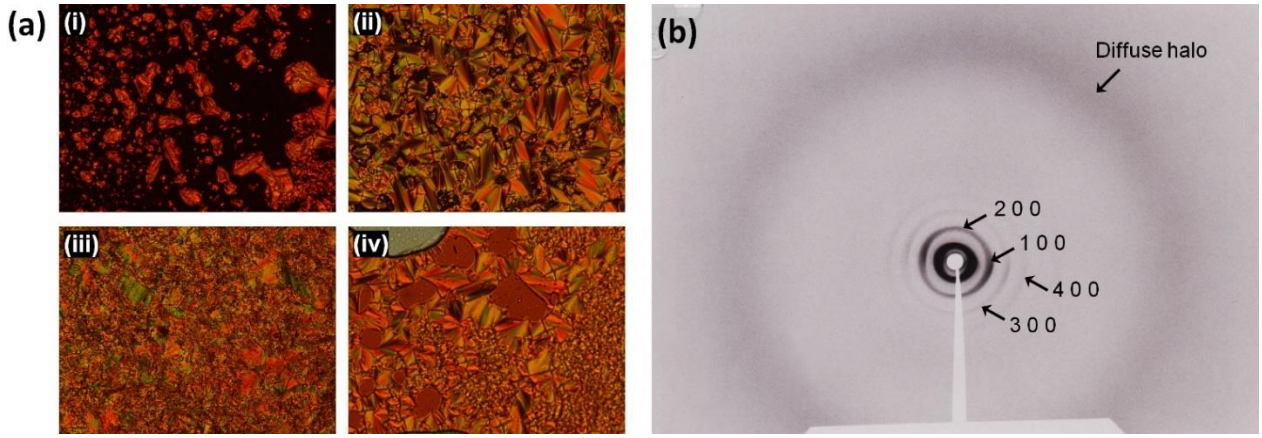

Figure 3. (a) POM textures of **calixAZO** taken at: i) 173°C in the first cooling, ii) 134°C in the first cooling, iii) 125°C in the second heating, iv) 165°C in the 2nd heating. **(b)** Room temperature XRD pattern of **calixAZO** in the glassy SmA mesophase.

Table 1. Thermal properties and structural parameters.

	$T_{5\%}$ (°C)[a]	Phase Transitions[b]	d_{obs}[d]	XRD parameters[e]
calixAZO	258	SmA_g 55 SmA 165[e] I	51.9	d = 52.1 Å
			26.0	S = 149.1 Å^2
			17.3	S_{ch} = 37.3 Å^2
			13.2	
			4.6 (br)	

[a] 5% mass loss temperature determined by TGA.
[b] DSC thermal transitions corresponding to the second heating scan (10 °C·min^{-1}). Temperatures (°C) are taken from the corresponding peak maximum. I: isotropic liquid, SmA: smectic A mesophase, SmA_g: glassy smectic A mesophase.
[c] POM data
[d] Experimental d value obtained from XRD (Å).
[e] d: layer spacing of the smectic phase (Å), S: estimated molecular cross-sectional area (Å^2), S_{ch}: estimated cross-sectional area per chain (Å^2)

Although the POM textures are characteristic of a SmA mesophase, the absolute assignment of the mesophase was achieved by X-ray diffraction (XRD). Prior to the XRD measurements, the sample was heated up to the isotropic liquid and cooled down to room temperature. The XRD patterns confirmed that the freezing of the mesophase and that crystallization did not occur. Temperature-dependent XRD measurements were also carried out, significant differences were not observed in the XRD patterns nor in the structural parameters of the mesophase.

The XRD patterns of **calixAZO** contained in the low-angle region a set of four equally spaced sharp, strong maxima that can be assigned respectively to the first, second, third and fourth order reflections from a lamellar structure (**Figure 3b**). In the high-angle region a broad, diffuse halo was detected that is related to the conformational disorder of the liquid-like alkyl chains. This kind of XRD pattern is characteristic of a lamellar mesophase which has been assigned as a smectic A organization, given the optical textures observed by POM. A layer spacing (d) of 52.1 Å was deduced by applying the Bragg's law to the small angle maxima. This d value is significantly larger than the molecule length in its most extended conformation (38.3 Å) suggesting that the mesophase adopts a bilayer structure.

Additional support for this bilayered structural model can be obtained by simple cross-section calculations. The density (ρ) of a smectic mesophase is related to the molecular mass (M) and the layer spacing (d) by the formula:

$$\rho = (M \times Z \times 10^{24})/(d \times S \times N_A)$$

where Z is the number of molecules per layer (Z=1 for a monolayer and Z=2 for a bilayer), S is the molecule cross-section, and N_A is Avogadro's number. Assuming ρ = 1 g·cm^{-3} (reasonable value for liquid crystals), it is deduced that in the case of a monolayer structure one molecule (Z=1) would fill a layer area (S) of about 74.5 Å^2. This would give a cross-section of 18.6 Å^2 per hydrocarbon chain, a value too narrow considering that the alkyl chains are conformationally disordered in the mesophase and 20 Å^2 would be the cross-section expected for a fully-extended all-*anti* hydrocarbon chain. The mesophase must therefore have a bilayer structure (Z=2) that, with the aforementioned formula, gives a molecule cross-section of 149.1 Å^2, i.e., 37.3 Å^2 per chain assuming both a head-to-head and cyano-to-cyano association of two calixarene molecules. This value may seem too large at first, but it can be rationalized by the conformational disorder of the hydrocarbon chains and by the interpenetration between the chains of molecules in neighboring layers. In the proposed bilayer structure, the molecules form two sublayers with an opposite orientation: in each sublayer the narrow rim of the molecules, containing the decyloxy groups directly bonded to the macrocycle, must be oriented towards the interior of the layer, whereas the wide rim, which contains the azobenzene moieties, must be oriented towards the surface (**Figure 4**). In this way, segregation of the different regions of the molecules takes place along the layer normal. This bilayer arrangement has been previously observed in other calixarene derivatives with smectic mesophases.[7, 38]

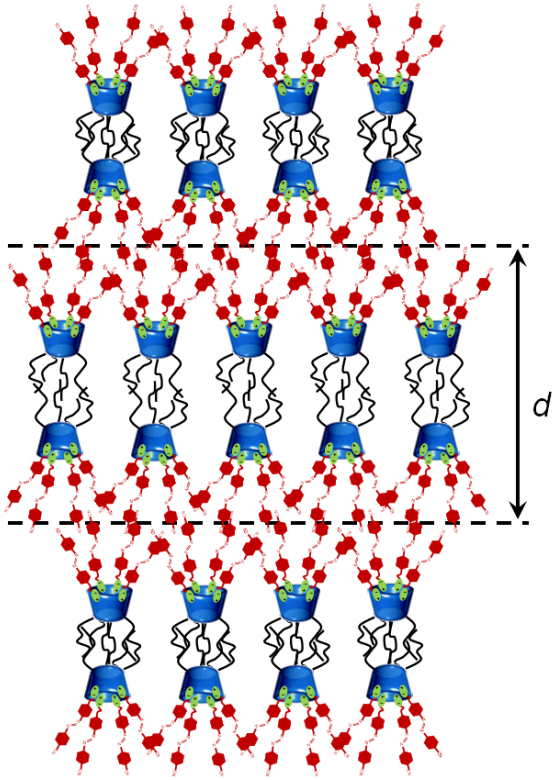

Figure 4. Proposed arrangement in the SmA LC phase.

The optical properties of **calixAZO** were investigated by UV-vis spectra for ~10^{-5} M solutions in THF. Additionally, films of **calixAZO** were obtained by casting THF solutions onto clean quartz substrates. The films were heated at 175 °C for 1 min and then rapidly cooled down to room temperature for sample homogenization purposes. **calixAZO** show an intense band at 365 nm related to the π–π* transition together with a weak absorption band about 450 nm corresponding to the symmetry forbidden n–π* transition of the *E*-cyanoazobenzene unit (**Figure 5a**). The as-casted films of **calixAZO** presented scattering and low-quality UV-vis spectra were obtained. After thermal treatment, the main π–π* absorption band is clearly broadened, when compared to THF solution, due to aggregation of the azobenzene moieties.

Exposure of **calixAZO** film to 365 nm UV irradiation caused *E* to *Z* photoisomerisation of the azobenzene units, and this was consistent with the remarkable decrease of the π–π* band and simultaneous increase of the absorbance at 450 nm. 15 min after light irradiation only slight changes were further detected in the UV-vis spectra. 24 h after UV light exposure, absorbance at around 365 nm increased and recovered the initial shape, indicating *Z*-to-*E* photoisomerization. This thermal isomerization is slow (hours scale) but can be accelerated by exposure to visible light. Thus, isomerized films were irradiated at 450 nm, and after 15 min the spectrum also recovered the initial shape (**Figure 5a**).

The proton conductivity was measured using electrochemical impedance spectroscopy (EIS) in samples consisting of films sandwiched between ITO-coated electrodes. The typical EIS response (Nyquist plots) consisted of a suppressed semicircle in the high-frequency region and an incline straight line in the low-frequency range. Since diffusible ions apart from protons did not exist in the compounds, the observed EIS response was ascribed to proton conduction, which was calculated from the EIS responses and the cell constant (see Experimental Part). The proton conductivities of **calixAZO** were measured as a function of temperature. These proton conductivities increase upon increasing the temperature from 30 °C to 175 °C (**Figure 5b**). In spite of exhibiting a smectic mesophase, **calixAZO** showed a very low proton conductivity in the whole temperature range. This result can be understood by keeping in mind the macrocyclic structure of **calixAZO** that precludes the interactions between the neighboring ionic pairs (proton-conductive active units) as they are located in the wide rim, thereby increasing the hopping distances.

It is noteworthy that after UV irradiation for 30 min the proton conductivities were reduced about two-orders of magnitude (**Figure 5b**). Upon UV irradiation, the elongated and thermodynamically stable *E* isomer suffers a reversible and fast change into the bent-shaped *Z* isomer. The calamitic (rod-like) structure of the *E* isomer is in the origin of the liquid crystalline properties usually reported in most of the azobenzene-containing materials. Therefore, the UV light-induced isomerization of azobenzene moieties resulted in a disturbance in the smectic mesophase that increases the mean effective hopping distances, decreasing the proton conductivity. This disturbance in the smectic mesophase can be canceled out by *Z*-to-*E* isomerization of azobenzene moieties, almost restoring the proton conductivity initial value (**Figure 5b**).

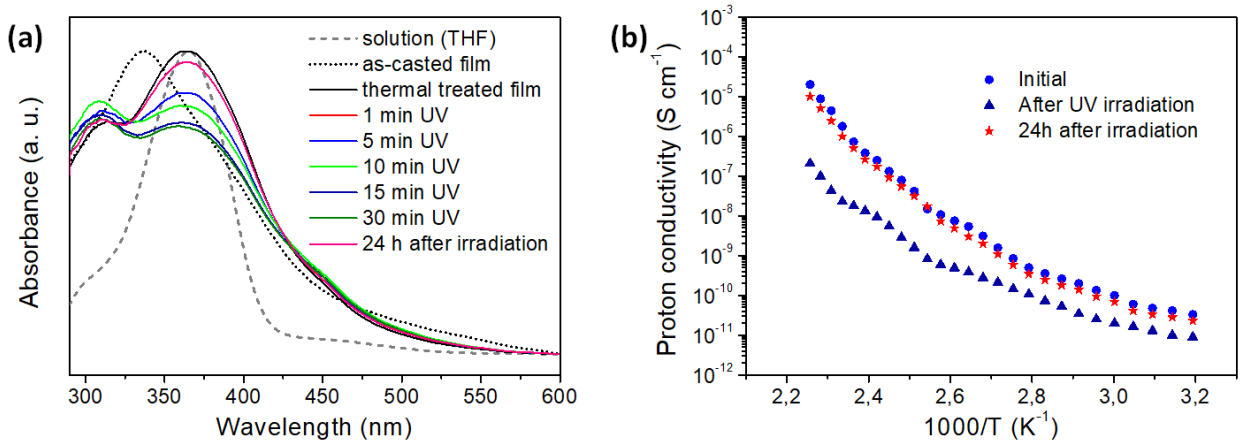

Figure 5. (a) Normalized UV-Vis absorption spectra. **(b)** Proton conductivities as a function of the temperature.

Conclusions

In conclusion, we have prepared an ionic LC that consists of a calix[4]arene core functionalized with azobenzene moieties via electrostatic self-assembly. In the solid state, the ionic calixarene undergoes microphase separation at the nanoscale, resulting in a lamellar LC organization (smectic A). The presence of the ionic salts is essential in this self-assembly process since the segregation between apolar and polar parts of the molecule is the driving force for the formation of the smectic LC phase. Moreover, this ionic LC calixarene showed proton conductive properties as the LC arrangement leads to the presence of ionic nanosegregated areas (formed by the ion pairs) that favor proton conduction. The presence of peripheral azobenzene units in the ionic LC provides light-responsive properties. Upon UV irradiation the elongated *E*-isomer suffers a reversible and fast change into the bent-shaped *Z*-isomer that leads to a disruption of the LC phase, thereby decreasing the proton conductivity values. This photo-isomerization is totally reversible and enables unique photo-switchable proton conductive properties.

Experimental Section

Materials

5-(*p*-Cyanophenylazophenyloxy)pentanoic acid (**Ac-AZO**) and 5,11,17,23-tetraamino-25,26,27,28-tetradecyloxycalix[4]arene (**calix(NH$_2$)$_4$**) were synthesized following previously reported procedures.[7, 37] All reagents were purchased from Sigma-Aldrich and used as received without further purification. Anhydrous tetrahydrofuran (THF) was purchased from Scharlab (analytical quality) and dried using a solvent purification system.

*Preparation of ionic **calixAZO***

calixAZO was prepared following the previously described methodology to prepare ionic liquid crystals.[35-36] A solution of **Ac-AZO** in dry THF was added to a dry THF solution of **calix(NH$_2$)$_4$**, in approximately 1:1 (primary amine groups:carboxylic acid groups) stoichiometry. The mixture was ultrasonicated for 10 min, and then it was slowly evaporated at room temperature and dried in vacuum at 40 °C until the weight remained constant.

Characterization Techniques

NMR experiments were carried out on Bruker Avance spectrometers operating at 400 MHz for ^{1}H and 100 MHz for ^{13}C, using standard pulse sequences. Chemical shifts are given in ppm relative to TMS and this was used as internal reference.

Mesogenic behavior was investigated by polarized-light optical microscopy (POM) using an Olympus BH-2 polarizing microscope fitted with a Linkam THMS600 hot stage. Thermogravimetric analysis (TGA) was performed using a Q5000IR from TA instruments at heating rate of 10 ºC min^{-1} under a nitrogen atmosphere. Thermal transitions were determined by differential scanning calorimetry (DSC) using a DSC Q2000 from TA instruments with powdered samples (2−5 mg) sealed in aluminum pans. Glass transition temperatures (T_g) were determined at the half height of the baseline jump, and first order transition temperatures were read at the maximum of the corresponding peak.

XRD experiments were performed in a pinhole camera (Anton-Paar) operating with a point-focused Ni-filtered Cu-Kα beam. Lindemann glass capillaries with 0.9 mm diameter were used to contain the sample. The capillary axis was placed perpendicular to the X-ray beam and the pattern was collected on flat photographic film perpendicular to the X-ray beam. Bragg's law was used to obtain the spacing.

UV-vis absorption spectra were measured with a UV4-200 from ATI-Unicam using 10^{-4}–10^{-5} M solutions in THF. Thin films for optical measurements were prepared by casting from THF solutions of the supramolecular polymers onto clean quartz substrates. The films were heated up to 175 ºC for 5 min and rapidly quenched to room temperature before performing the optical measurements. These films were irradiated with a compact low-pressure fluorescent lamp Philips PL-S 9W emitting between 350 and 400 nm. The samples were placed at a distance of 10 cm from the light source at room temperature.

Electrochemical impedance spectroscopy was recorded on an Autolab potentiostat equipped with a temperature controller in the frequency range from 1 Hz to 1 MHz (applied voltage: 10 mV). The conductivities were studied as a function of temperature between 30°C and 225°C at 5°C intervals. For the preparation of the cells for ionic conductivities, the appropriate amount of the ionic dendrimer was placed onto an ITO electrode that was sandwiched with another ITO electrode controlling the thickness by using glass spacers (20 µm). The cell was heated up to a few degrees above the melting point of the liquid crystal and the cell was pressed to obtain the thin film. The impedance spectrum can be modeled as an equivalent circuit and divided into imaginary (Z'') and real (Z') components. The resistance (R_b) was estimated from the intersection of the real axis (Z') and the semicircle of the impedance spectrum. The proton conductivities σ (S·cm^{-1}) were calculated with the formula: $\sigma = d / (R_b \cdot A)$), where d (cm) is the thickness of the film, A (cm^2) is the area of the film and R_b (Ω) is the resistance of the sample.

Acknowledgements

This work was supported by the MCIU/AEI/FEDER-UE funds (PGC2018-097583-B-I00 and PID2021-122882NB-I00), and Gobierno de Aragón-FSE (Research Group E47_17R). A. C. thanks the "Ramón y Cajal Program" (Grant No. RYC2021-031154-I) funded by MCIN/AEI/10.13039/501100011033 and EU-"NextGenerationEU"/PRTR. Authors would like to acknowledge the use of the SAI (UZ) and CEQMA (UZ-CSIC) Services.

Author Contribution Statement

M.M. and J.L.S. conceived and designed the experiments. A.C. and I.M. performed the experiments and analyzed the data. J.B, M.M. and J.L.S. analyzed the data and supervised the work. A.C. and J.L.S wrote the manuscript.

References

1. S. Sameni, C. Jeunesse, D. Matt, J. Harrowfield. 'Calix[4]arene daisychains'. *Chem. Soc. Rev.* **2009,** *38* (7), 2117-2146.
2. F. Zhang, Y. Sun, D. Tian, W. S. Shin, J. S. Kim, H. Li. 'Selective molecular recognition on calixarene-functionalized 3D surfaces'. *Chem. Commun.* **2016,** *52* (86), 12685-12693.

3. H. J. Kim, M. H. Lee, L. Mutihac, J. Vicens, J. S. Kim. 'Host–guest sensing by calixarenes on the surfaces'. *Chem. Soc. Rev.* **2012,** *41* (3), 1173-1190.
4. R.-Q. Lu, S.-X. L. Luo, Q. He, A. Concellón, T. M. Swager. 'Methane Detection with a Tungsten-Calix[4]arene-Based Conducting Polymer Embedded Sensor Array'. *Adv. Funct. Mater.* **2021,** *31* (6), 2007281.
5. F. Yang, H. Guo, J. Vicens. 'Mini-review: calixarene liquid crystals'. *Journal of Inclusion Phenomena and Macrocyclic Chemistry* **2014,** *80* (3), 177-186.
6. V. S. Sharma, V. K. Vishwakarma, P. S. Shrivastav, A. Ammathnadu Sudhakar, A. S. Sharma, P. A. Shah. 'Calixarene Functionalized Supramolecular Liquid Crystals and Their Diverse Applications'. *ACS Omega* **2022**, DOI: 10.1021/acsomega.2c04699.
7. J. Romero, J. Barberá, M. J. Blesa, A. Concellón, P. Romero, J. L. Serrano, M. Marcos. 'Liquid Crystal Organization of Calix[4]arene-Appended Schiff Bases and Recognition towards Zn^{2+}'. *ChemistrySelect* **2017,** *2* (1), 101-109.
8. V. S. Sharma, A. S. Sharma, N. K. Agarwal, P. A. Shah, P. S. Shrivastav. 'Self-assembled blue-light emitting materials for their liquid crystalline and OLED applications: from a simple molecular design to supramolecular materials'. *Molecular Systems Design & Engineering* **2020,** *5* (10), 1691-1705.
9. V. S. Sharma, A. P. Shah, A. S. Sharma, M. Athar. 'Columnar self-assembly, gelation and electrochemical behavior of cone-shaped luminescent supramolecular calix[4]arene LCs based on oxadiazole and thiadiazole derivatives'. *New. J. Chem.* **2019,** *43* (4), 1910-1925.
10. V. S. Sharma, A. S. Sharma, S. J. B. Worthington, P. A. Shah, P. S. Shrivastav. 'Columnar self-assembly, electrochemical and luminescence properties of basket-shaped liquid crystalline derivatives of Schiff-base-moulded p-tert-butyl-calix[4]arene'. *New. J. Chem.* **2020,** *44* (47), 20610-20619.
11. V. S. Sharma, A. S. Sharma, A. P. Shah, P. A. Shah, P. S. Shrivastav, M. Athar. 'New Class of Supramolecular Bowl-Shaped Columnar Mesogens Derived from Thiacalix[4]arene Exhibiting Gelation and Organic Light-Emitting Diodes Applications'. *ACS Omega* **2019,** *4* (14), 15862-15872.
12. B. Hong, F. Yang, H. Guo, Z. Jiao. 'Synthesis, complexation, and mesomorphism of novel calixarene-linked discotic triphenylene based on click chemistry'. *Tetrahedron Letters* **2014,** *55* (1), 252-255.
13. F. Yang, X. Bai, H. Guo, C. Li. 'Ion complexation-induced mesomorphic conversion between two columnar phases of novel symmetrical triads of triphenylene-calix[4]arene-triphenylenes'. *Tetrahedron Letters* **2013,** *54* (5), 409-413.
14. X. Fang, H. Guo, F. Yang, Y. Wu. 'Novel gallic-calixarene liquid crystals: syntheses and conformation influences on mesomorphism'. *Tetrahedron Letters* **2015,** *56* (44), 6128-6131.
15. H. Guo, F. Yang, W. Liu, J. Lai. 'Novel supramolecular liquid crystals: synthesis and mesomorphic properties of calix 4 arene-cholesterol derivatives'. *Tetrahedron Letters* **2015,** *56* (6), 866-870.
16. X. Zhang, H. Guo, F. Yang, J. Yuan. 'Ion complexation-controlled columnar mesophase of calix[4]arene–cholesterol derivatives with Schiff-base bridges'. *Tetrahedron Letters* **2016,** *57* (8), 905-909.
17. C. F. J. Faul. 'Ionic Self-Assembly for Functional Hierarchical Nanostructured Materials'. *Acc. Chem. Res.* **2014,** *47* (12), 3428-3438.
18. C. F. J. Faul, M. Antonietti. 'Ionic Self-Assembly: Facile Synthesis of Supramolecular Materials'. *Adv. Mater.* **2003,** *15* (9), 673-683.
19. A. Concellón, V. Iguarbe, Ionic Self-Assembly of Dendrimers. In *Supramolecular Assemblies Based on Electrostatic Interactions*, M. A. Aboudzadeh; A. Frontera, Eds. Springer International Publishing: Cham, 2022; pp 85-118.
20. K. Salikolimi, A. A. Sudhakar, Y. Ishida. 'Functional Ionic Liquid Crystals'. *Langmuir* **2020,** *36* (40), 11702-11731.
21. K. Goossens, K. Lava, C. W. Bielawski, K. Binnemans. 'Ionic Liquid Crystals: Versatile Materials'. *Chem. Rev.* **2016,** *116* (8), 4643-4807.
22. A. Concellón, M. San Anselmo, S. Hernández-Ainsa, P. Romero, M. Marcos, J. L. Serrano. 'Micellar Nanocarriers from Dendritic Macromolecules Containing Fluorescent Coumarin Moieties'. *Polymers* **2020,** *12* (12), 2872.
23. A. Concellón, T. Liang, A. P. H. J. Schenning, J. L. Serrano, P. Romero, M. Marcos. 'Proton-conductive materials formed by coumarin photocrosslinked ionic liquid crystal dendrimers'. *J. Mater. Chem. C* **2018,** *6* (5), 1000-1007.
24. A. Concellón, S. Hernández-Ainsa, J. Barberá, P. Romero, J. L. Serrano, M. Marcos. 'Proton conductive ionic liquid crystalline poly(ethyleneimine) polymers functionalized with oxadiazole'. *RSC Adv.* **2018,** *8* (66), 37700-37706.
25. M. Castillo-Vallés, M. Cano, A. Bermejo-Sanz, N. Gimeno, M. B. Ros. 'Towards supramolecular nanostructured materials: control of the self-assembly of ionic bent-core amphiphiles'. *J. Mater. Chem. C* **2020,** *8* (6), 1998-2007.
26. M. Cano, A. Sánchez-Ferrer, J. L. Serrano, N. Gimeno, M. B. Ros. 'Supramolecular Architectures from Bent-Core Dendritic Molecules'. *Angew. Chem. Int. Ed.* **2014,** *53* (49), 13449-13453.
27. A. Concellón, E. Blasco, A. Martínez-Felipe, J. C. Martínez, I. Šics, T. A. Ezquerra, A. Nogales, M. Piñol, L. Oriol. 'Light-Responsive Self-Assembled Materials by Supramolecular Post-Functionalization via Hydrogen Bonding of Amphiphilic Block Copolymers'. *Macromolecules* **2016,** *49* (20), 7825-7836.
28. H. K. Bisoyi, Q. Li. 'Light-Driven Liquid Crystalline Materials: From Photo-Induced Phase Transitions and Property Modulations to Applications'. *Chem. Rev.* **2016,** *116* (24), 15089-15166.
29. E. Blasco, M. Piñol, L. Oriol. 'Responsive linear-dendritic block copolymers'. *Macromol. Rapid Commun.* **2014,** *35* (12), 1090-1115.
30. E. Blasco, M. Piñol, L. Oriol, B. V. K. J. Schmidt, A. Welle, V. Trouillet, M. Bruns, C. Barner-Kowollik. 'Photochemical Generation of Light Responsive Surfaces'. *Adv. Funct. Mater.* **2013,** *23* (32), 4011-4019.
31. T. Ikeda, T. Ube. 'Photomobile polymer materials: from nano to macro'. *Mater. Today* **2011,** *14* (10), 480-487.
32. A. H. Gelebart, D. Jan Mulder, M. Varga, A. Konya, G. Vantomme, E. W. Meijer, R. L. B. Selinger, D. J. Broer. 'Making waves in a photoactive polymer film'. *Nature* **2017,** *546* (7660), 632-636.
33. H. P. C. van Kuringen, Z. J. W. A. Leijten, A. H. Gelebart, D. J. Mulder, G. Portale, D. J. Broer, A. P. H. J. Schenning. 'Photoresponsive Nanoporous Smectic Liquid Crystalline Polymer Networks: Changing the Number of Binding Sites and Pore Dimensions in Polymer Adsorbents by Light'. *Macromolecules* **2015,** *48* (12), 4073-4080.
34. D. Liu, D. J. Broer. 'Self-assembled Dynamic 3D Fingerprints in Liquid-Crystal Coatings Towards Controllable Friction and Adhesion'. *Angew. Chem. Int. Ed.* **2014,** *53* (18), 4542-4546.
35. R. Martín-Rapún, M. Marcos, A. Omenat, J. Barberá, P. Romero, J. L. Serrano. 'Ionic Thermotropic Liquid Crystal Dendrimers'. *J. Am. Chem. Soc.* **2005,** *127* (20), 7397-7403.
36. V. Chechik, M. Zhao, R. M. Crooks. 'Self-Assembled Inverted Micelles Prepared from a Dendrimer Template: Phase Transfer of Encapsulated Guests'. *J. Am. Chem. Soc.* **1999,** *121* (20), 4910-4911.
37. M. Marcos, R. Alcalá, J. Barberá, P. Romero, C. Sánchez, J. L. Serrano. 'Photosensitive ionic nematic liquid crystalline complexes based on dendrimers and hyperbranched polymers and a cyanoazobenzene carboxylic acid'. *Chem. Mater.* **2008,** *20* (16), 5209-5217.
38. T. Gu, G. Accorsi, N. Armaroli, D. Guillon, J.-F. Nierengarten. 'Calix[4]oligophenylenevinylene: a new rigid core for the design of π-conjugated liquid crystalline derivatives'. *Tetrahdron Lett.* **2001,** *42* (12), 2309-2312.